

A synthetic gauge field for two-dimensional time-multiplexed quantum random walks

Hamidreza Chalabi,^{*} Sabyasachi Barik,[†] Sunil Mittal,[‡] Thomas E. Murphy,[§] Mohammad Hafezi,[¶] and Edo Waks^{**}
*Department of Electrical and Computer Engineering,
 The University of Maryland at College Park, College Park, MD 20742, USA*

Temporal multiplexing provides an efficient and scalable approach to realize a quantum random walk with photons that can exhibit topological properties. But two dimensional time-multiplexed topological quantum walks studied so far have relied on generalizations of the Su-Shreiffer-Heeger (SSH) model with no synthetic gauge field. In this work, we demonstrate a 2D topological quantum random walk where the non-trivial topology is due to the presence of a synthetic gauge field. We show that the synthetic gauge field leads to the appearance of multiple bandgaps and consequently, a spatial confinement of the random walk distribution. Moreover, we demonstrate topological edge states at an interface between domains with opposite synthetic fields. Our results expand the range of Hamiltonians that can be simulated using photonic random walks.

Photonics provides a compelling platform to study quantum random walks [1]. Photons can propagate over long distances without losing coherence, enabling complex random walks that can implement various quantum computing algorithms [2–4], and also simulate a broad range of quantum Hamiltonians [5]. Photonic random walks in both one and two dimensions can be implemented in spatial degrees of freedom using beam splitters [6–8] or coupled waveguide arrays [9–11]. But such approaches are difficult to scale to large number of steps, particularly when going to higher dimensions.

Synthetic spaces provide an alternative approach to scale the state-space of the walker without requiring complex photonic circuits. Examples of synthetic spaces include frequency [12–16], orbital angular momentum [17–20], and transverse spatial modes as recently experimentally realized [21]. Time-multiplexing is another synthetic space that is particularly easy to work with [22–27]. Time-multiplexed random walks have the advantage that they can span an extremely large state-space with only a few optical elements and can efficiently scale to higher number of walker dimensions.

Recently, time-multiplexed quantum walks have been used to explore topological physics and the associated edge states in both one and two dimensional systems [26, 27]. Most realizations of such topological quantum walks are based on the split-step quantum walk protocol [28–31]. Similar to the Su-Shreiffer-Heeger (SSH) model, here the non-trivial topology is a result of the direction-dependent hopping strength between the lattice sites. However, many of the most interesting topological Hamiltonians, such as the integer quantum Hall effect [32], the Haldane model [33], and the quantum-spin Hall effect [34], require gauge fields that generate direction-dependent hopping phases. So far, time-multiplexed random walks with synthetic gauge fields have only been implemented in 1D, which severely restricts the number of topological Hamiltonians that can be explored.

Here, we demonstrate a two-dimensional topological synthetic gauge field in a time-multiplexed quantum walk. We show that in our discrete-time quantum

walk, the pseudo-energy band structure exhibits multiple bandgaps depending on the magnitude of the synthetic gauge field. These bandgaps result in the confinement of the random walker, as opposed to ballistic diffusion that would otherwise occur [35]. Moreover, we demonstrate the presence of multiple topological edge bands at an interface between two domains with opposite magnetic fields. Because of the presence of two topological edge bands, our system supports two sets of non-degenerate topological edge states that travel in forward and backward directions along the interface.

To implement a gauge field, pulses must accumulate a net phase shift when walking around a closed trajectory. Figure 1a shows how we implement this condition. We apply a phase shift of $y\phi$ when the walker moves to the right, and $-y\phi$ when the walker steps to the left, where y is the vertical coordinate of the walker. This phase convention realizes a uniform magnetic field in the Landau gauge. Consequently, this phase modulation scheme can be harnessed as an artificial gauge field affecting the evolution of the random walk.

In our time-multiplexed photonic random walk, optical delays map the walker state-space into time-delays of optical pulses. Similar to earlier studies [24, 27] of two dimensional quantum random walks, we implement these delays using a pair of nested fiber delay loops. Figure 1b shows the schematic of the experimental setup, and the full details are explained in the Supplementary Material [36]. The experimental setup essentially consists of two beam-splitters with their ports connected to fibers of different lengths such that they map the $\pm x$ and $\pm y$ directions to different time delays. One complete propagation of an optical pulse around the loop is then equivalent to hopping of the walker to one of the four possible corners in the synthetic space (Fig. 1a). Two semiconductor optical amplifiers (SOAs) are employed to partially compensate for the losses that the optical pulses experience in each round trip. In this setup, we study the random walk distribution at each time step via two photodetectors analyzing two channels that we refer to as the up and down channels as labeled in Fig. 1b.

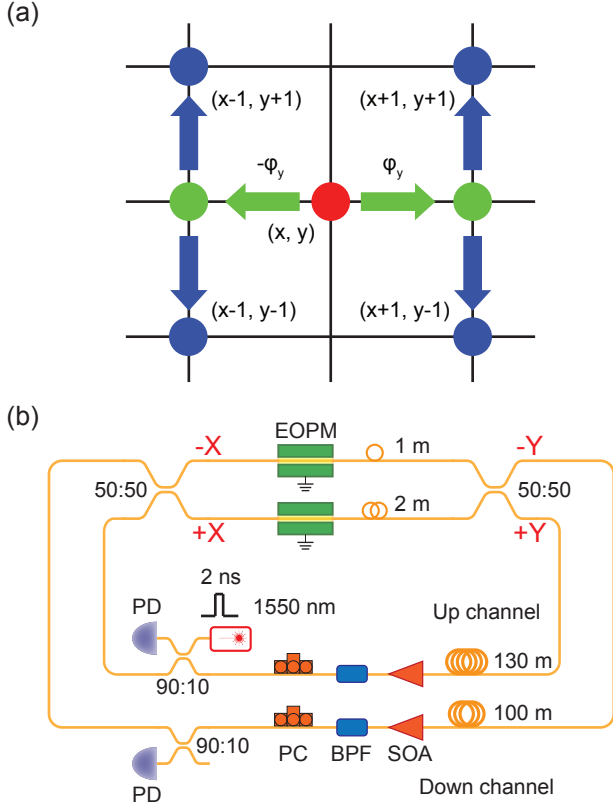


Figure 1. (a) Schematic explaining the possible movements of a walker at spatial position (x, y) along with applied phase shifts during each step of the random walk. (b) Schematic of the 2D random walk setup describing the details of the experimental setup. PD: photodetector, BPF: band pass filter, SOA: semiconductor optical amplifier, EOPM: electro-optic phase modulator, and PC: polarization controller.

We initialize the random walk through a single incident laser pulse that is injected into the up channel starting the evolution of random walk distribution from the origin in synthetic space. Here, we have analyzed the evolution of the random walk based on the pulses detected in the down channel. The electro-optic modulators which are driven by programmable voltage waveforms are used for producing the desired phase shifts to generate the synthetic gauge field.

Figure 2 compares the evolution of the random walk distribution with and without an applied gauge field. Figure 2a shows the experimental results for the evolution under no applied gauge field. In this figure, the distribution of the random walker is shown at three different time steps of 1, 5, and 9. In the absence of a gauge field, the random walk exhibits rapid diffusion. These results are consistent with the theoretical predictions shown in Fig. 2b. Figure 2c shows the experimental results for the evolution of the random walk distribution in the presence of a gauge field with $\phi = \pi/2$. The gauge field leads to

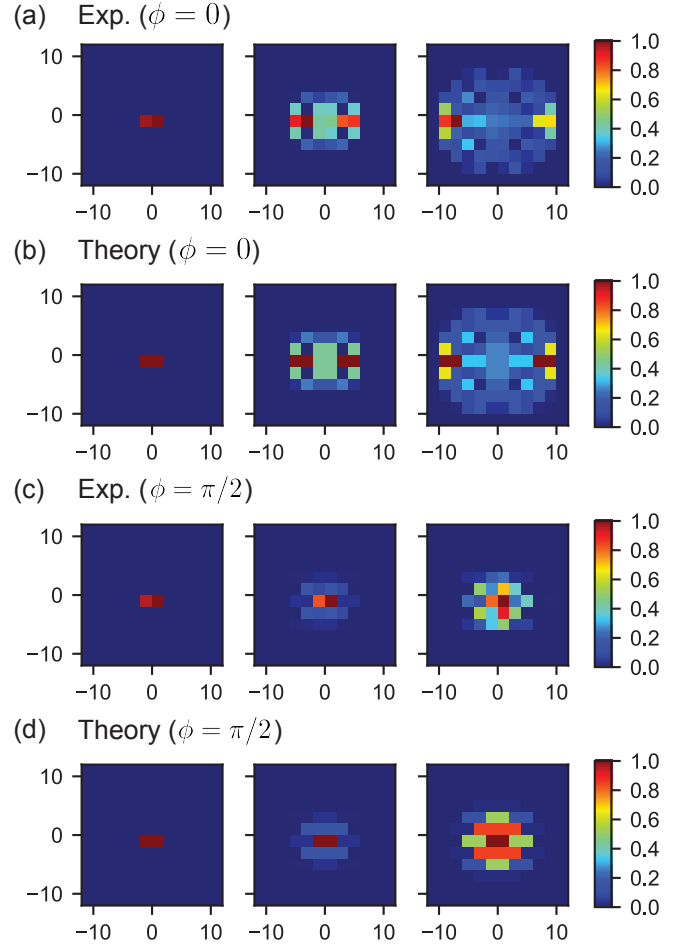


Figure 2. (a) Experimental observations and (b) theoretical predictions of the evolution of the random walk distribution under no phase modulation. (c) Experimental observations and (d) theoretical predictions of the evolution of the random walk distribution under linearly dependent phase modulation $\phi_y = y\phi$ for the case of $\phi = \pi/2$. The left, middle, and right columns show the distributions at time steps of 1, 5, and 9, respectively. In these plots all the distributions are normalized to their maximum.

suppressed diffusion and confinement of the random walk distribution. The experimental results shown in Fig. 2c for the case of a gauge field with $\phi = \pi/2$ are consistent with the theoretical predictions shown in Fig. 2d.

We calculate the fidelity of the measured distributions relative to the theoretical distributions (P_{th}) based on $F(n) = \sum_{x,y} \sqrt{P_{th}(x,y;n)} P_{exp}(x,y;n)$. For the case of no applied gauge field, we obtained fidelities of 0.999, 0.996, and 0.985 for time steps of 1, 5, and 9, respectively. Similarly, for the random walk under the gauge field we determined fidelities of 0.999, 0.993, and 0.972 for time steps of 1, 5, and 9, respectively.

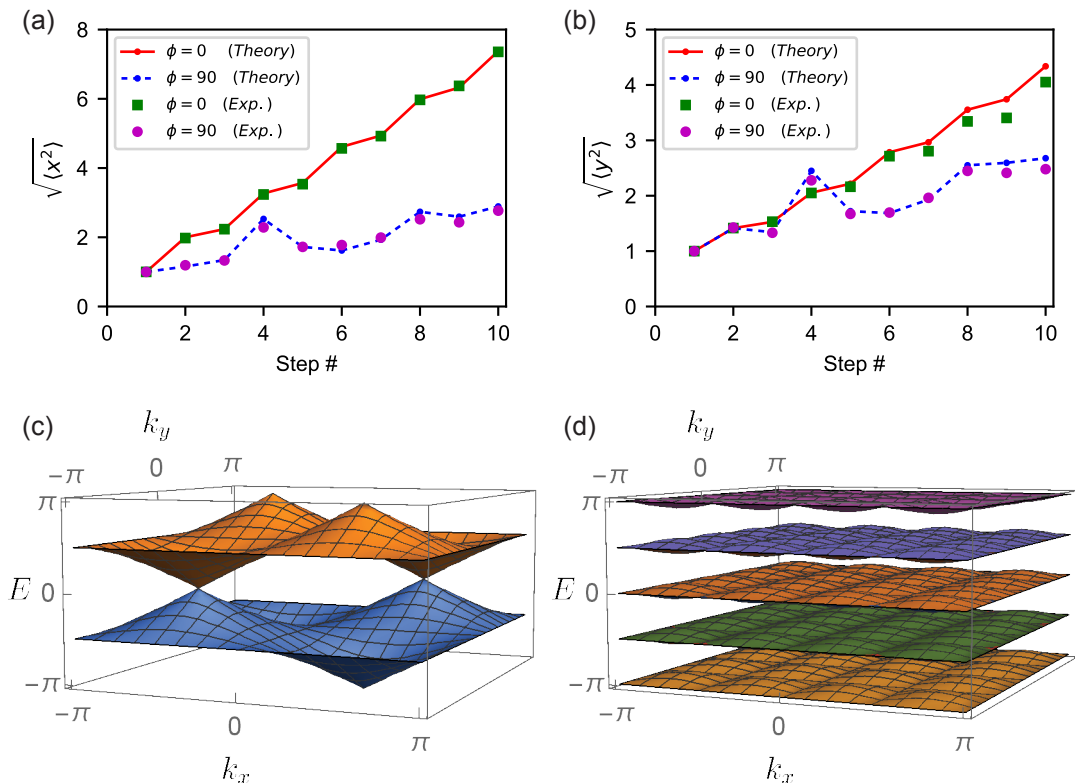


Figure 3. (a) Comparison of the theoretical and experimental results for the variation of the random walk distribution quadratic mean in the x direction under no gauge field as well as under the gauge field with $\phi = \frac{\pi}{2}$. (b) Comparison of the theoretical and experimental results for the variation of the random walk distribution quadratic mean in the y direction under no gauge field as well as under the gauge field with $\phi = \frac{\pi}{2}$. (c, d) Band structure of the system under no phase modulation ($\phi = 0$) and a linear phase modulation ($\phi = \frac{\pi}{2}$).

To provide a more quantitative analysis of the effect of the gauge field on the particle confinement, we calculate the variation of the spatial quadratic means of the random walk distribution as a function of time step. Figures 3a and 3b plot the quadratic means in the x and y directions with gauge fields of $\phi = 0$ and $\phi = \pi/2$. With no applied gauge field, the quadratic means show nearly linear variation with the time step, consistent with ballistic diffusion (See Supplementary Material [36] for analytical explanation). But under the application of the gauge field with $\phi = \pi/2$, the quadratic means show reduced diffusion. The decrease of the quadratic means in both directions is due to the confinement of the random walk's distribution under a constant pseudo magnetic field. Figures 3a and 3b confirm the agreement of the experimental results with the theoretical predictions, both with and without the effect of the gauge field. (See also Fig. S3 for the numerical study of the variation of quadratic means over a larger number of steps)

In order to better understand the confinement of the random walker in the presence of a gauge field, we first calculate the band structure of the random walk. The full evolution of the walker is determined by the single-

step propagation matrix U , which advances the random walker distribution by one time-step. According to Floquet band theory, the single-step propagation matrix determines the effective Hamiltonian from $U = e^{-iH_{eff}}$, which gives the band structure of the walker. With no synthetic gauge field ($\phi = 0$), we can analytically solve for the dispersion relation of the walker (See theoretical analysis section in the Supplementary Material [36]). The quasi-energy bands of the system in this case are

$$E_{\pm} = \pm \arccos(\sin(k_x) \sin(k_y)), \quad (1)$$

where k_x and k_y are the momentum wave vectors in inverse synthetic space. Figure 3c shows the corresponding band structure of the system. Because of the discrete nature of the random walk, the quasi-energy spectrum wraps every 2π , and therefore we restrict the quasi-energies to the range of $-\pi$ and π . As Fig. 3c shows, the system is gapless, and there are four Dirac points, two at $E = 0$ and two at $E = \pm\pi$.

We next consider the effect of the synthetic gauge field on the band structure. Figure 3d shows the band diagram for the case of $\phi = \frac{\pi}{2}$. An analytical solution for this

case also exists (see Supplementary Material [36]), with a quasi-energy band structure given by

$$E_{n,\pm} = \frac{n\pi}{2} \pm \frac{1}{4} \arccos \left(1 - \frac{1}{2} \sin^2(2k_x) \sin^2(2k_y) \right) \quad (2)$$

for $n \in \mathbb{Z}$. Similar to the case of integer quantum Hall effect, the introduction of a gauge field produces a series of topological bands. For $\phi = \frac{\pi}{2}$, we observe four doubly degenerate bands. However, because of the wrapping of pseudo-energy, one set of bands is split and appears close to energies $\pm\pi$. In contrast to the zero gauge field, the band structure in the presence of a synthetic gauge field exhibits bandgaps that lead to the confinement of the random walker. We have also obtained the corresponding band diagrams for several other choices of ϕ . We have presented these results (See Fig. S2) along with their derivation in the Supplementary Material [36].

One consequence of a gauge field is the presence of edge states at the boundaries. In this synthetic space, we can make a boundary by applying two different gauge fields to two neighboring regions. Here, using a phase modulation pattern of $\phi_y = y\phi$ for $y > 0$ and $\phi_y = -y\phi$ for $y < 0$, we realize two domains with opposite magnetic fields ($y > 0$ and $y < 0$), as illustrated in Fig. 4a. Figure 4b shows the band structure for such a phase pattern with $\phi = \frac{\pi}{2}$. The band diagram contains multiple bandgaps hosting unidirectional edge states that propagate at the boundary in opposite directions. The corresponding band diagrams for several other choices of ϕ are also presented in the Supplementary Material [36](See Fig. S4).

Figure 4c shows experimentally measured results for the phase modulation pattern shown in Fig. 4a. We start the random walker at the interface between the two magnetic domains, precisely where edge states should be present. In this case the random walker predominantly walks along the edge, remaining confined to the boundary between the two regions. These results are consistent with the numerical simulations demonstrating how the edge states cause the random walk distribution to move mainly along the boundary (Fig. 4d).

Typical topological quantum walks result in unidirectional edge state propagation. Here, however, we do not see unidirectional movements because we are initializing the walker at a position eigenstate, which is a superposition of all energy eigenstates of the band structure. As can be seen from Fig. 4b, different energy bands support topological edge states propagating in either the left or right direction. We could excite specific edge modes by engineering the initial distribution of the random walk to be confined in corresponding energies. Additionally, more complicated phase modulation patterns can be harnessed to produce sharp edges in the synthetic space.

In conclusion, we have implemented time-multiplexed two-dimensional quantum random walks with a synthetic gauge field. This gauge field leads to the confinement

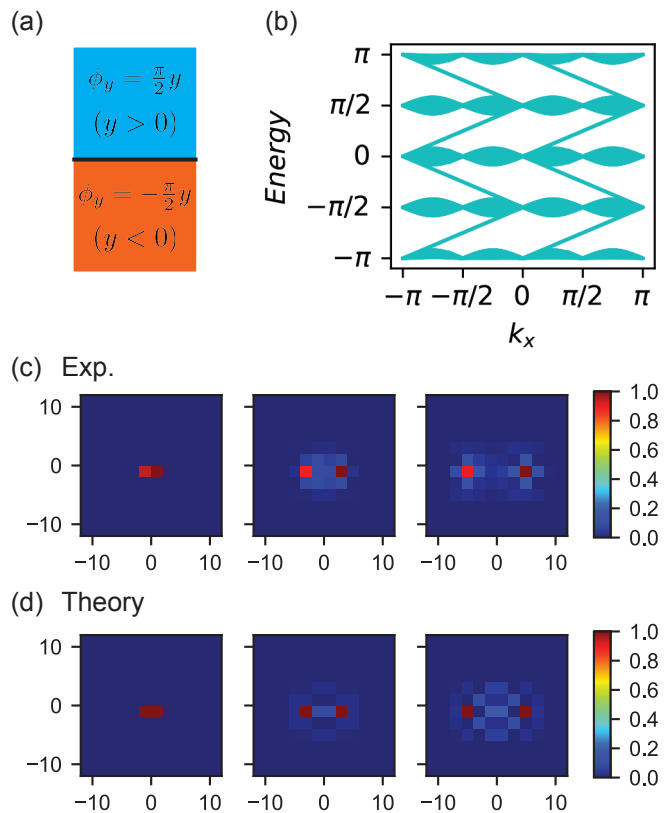


Figure 4. (a) The schematic describing the phase modulation pattern of $\phi_y = |y|\phi$ for $\phi = \frac{\pi}{2}$ in the synthetic space. (b) Band diagram of the corresponding system which clearly shows the presence of edge states in the bandgap. (c) Experimental observations and (d) theoretical predictions of the evolution of the random walk distribution moving along the boundary under the phase modulation of $\phi_y = |y|\phi$ for $\phi = \frac{\pi}{2}$. The left, middle, and right columns show the distributions at time steps of 1, 5, and 9, respectively. In these plots all the distributions are normalized to their maximum.

of the walker evolution. Through application of an inhomogeneous gauge field on this random walk, we observed the creation of topological edge states that are confined at the boundary of two distinct gauge fields. These results demonstrate a versatile approach to create various types of band structures with tunable number of bandgaps. In order to increase the number of steps, we used optical amplifiers to compensate for round-trip losses without damaging the phase coherence of the optical pulses. These losses can be reduced by decreasing coupler losses through fiber splicing and the use of modulators with lower insertion loss. Eliminating these losses opens up a path towards quantum random walks that can be implemented at the single photon level, or in higher dimensions. Addition of optical nonlinearities and integration of this platform with single photon emitters could provide another interesting opportunity to study topo-

logical band structures with optical interactions [37, 38]. Ultimately, our results expand the toolbox of quantum photonic simulation and provide a scalable architecture to study photonic random walks with non-trivial topologies.

This work was supported by the Air Force Office of Scientific Research-Multidisciplinary University Research Initiative (Grant FA9550-16-1-0323), the Physics Frontier Center at the Joint Quantum Institute, the National Science Foundation (Grant No. PHYS. 1415458), and the Center for Distributed Quantum Information. The authors would also like to acknowledge support from the U.S. Department of Defense.

* hchalabi@umd.edu

† sbarik@umd.edu

‡ smittal@umd.edu

§ tem@umd.edu

¶ hafezi@umd.edu

** edowaks@umd.edu

- [1] Y. Aharonov, L. Davidovich, and N. Zagury, *Physical Review A* **48**, 1687 (1993).
- [2] J. Kempe, *Contemporary Physics* **44**, 307 (2003).
- [3] N. Shenvi, J. Kempe, and K. B. Whaley, *Physical Review A* **67**, 052307 (2003).
- [4] A. M. Childs, R. Cleve, E. Deotto, E. Farhi, S. Gutmann, and D. A. Spielman, in *Proceedings of the thirty-fifth ACM symposium on Theory of computing - STOC '03* (ACM Press, New York, New York, USA, 2003) p. 59.
- [5] A. M. Childs, D. Gosset, and Z. Webb, *Science (New York, N.Y.)* **339**, 791 (2013).
- [6] F. De Nicola, L. Sansoni, A. Crespi, R. Ramponi, R. Osellame, V. Giovannetti, R. Fazio, P. Mataloni, and F. Sciarrino, *Physical Review A* **89**, 032322 (2014).
- [7] L. Sansoni, F. Sciarrino, G. Vallone, P. Mataloni, A. Crespi, R. Ramponi, and R. Osellame, *Physical Review Letters* **108**, 010502 (2012).
- [8] M. A. Broome, A. Fedrizzi, B. P. Lanyon, I. Kassal, A. Aspuru-Guzik, and A. G. White, *Physical Review Letters* **104**, 153602 (2010).
- [9] K. Poulios, R. Keil, D. Fry, J. D. A. Meinecke, J. C. F. Matthews, A. Politi, M. Lobino, M. Gräfe, M. Heinrich, S. Nolte, A. Szameit, and J. L. O'Brien, *Physical Review Letters* **112**, 143604 (2014).
- [10] H. Tang, X.-F. Lin, Z. Feng, J.-Y. Chen, J. Gao, K. Sun, C.-Y. Wang, P.-C. Lai, X.-Y. Xu, Y. Wang, L.-F. Qiao, A.-L. Yang, and X.-M. Jin, *Science Advances* **4**, eaat3174 (2018).
- [11] H. Tang, C. Di Franco, Z.-Y. Shi, T.-S. He, Z. Feng, J. Gao, K. Sun, Z.-M. Li, Z.-Q. Jiao, T.-Y. Wang, M. S. Kim, and X.-M. Jin, *Nature Photonics* **12**, 754 (2018).
- [12] C. Navarrete-Benlloch, A. Pérez, and E. Roldán, *Physical Review A* **75**, 062333 (2007).
- [13] D. Bouwmeester, I. Marzoli, G. P. Karman, W. Schleich, and J. P. Woerdman, *Physical Review A* **61**, 013410 (1999).
- [14] Q. Lin, M. Xiao, L. Yuan, and S. Fan, *Nature Communications* **7**, 13731 (2016).
- [15] Q. Lin, X.-Q. Sun, M. Xiao, S.-C. Zhang, and S. Fan, *Science Advances* **4**, eaat2774 (2018).
- [16] L. Yuan, M. Xiao, Q. Lin, and S. Fan, *Physical Review B* **97**, 104105 (2018), arXiv:1710.01373.
- [17] S. K. Goyal, F. S. Roux, A. Forbes, and T. Konrad, *Physical Review Letters* **110**, 263602 (2013).
- [18] F. Cardano, F. Massa, H. Qassim, E. Karimi, S. Slusarenko, D. Paparo, C. de Lisio, F. Sciarrino, E. Santamato, R. W. Boyd, and L. Marrucci, *Science Advances* **1**, e1500087 (2015).
- [19] F. Cardano, M. Maffei, F. Massa, B. Piccirillo, C. de Lisio, G. De Filippis, V. Cataudella, E. Santamato, and L. Marrucci, *Nature Communications* **7**, 11439 (2016).
- [20] F. Cardano, A. D'Errico, A. Dauphin, M. Maffei, B. Piccirillo, C. de Lisio, G. De Filippis, V. Cataudella, E. Santamato, L. Marrucci, M. Lewenstein, and P. Massignan, *Nature Communications* **8**, 15516 (2017).
- [21] E. Lustig, S. Weimann, Y. Plotnik, Y. Lumer, M. A. Bandres, A. Szameit, and M. Segev, (2018), arXiv:1807.01983.
- [22] A. Schreiber, K. N. Cassemiro, V. Potoček, A. Gábris, P. J. Mosley, E. Andersson, I. Jex, and C. Silberhorn, *Physical Review Letters* **104**, 050502 (2010).
- [23] A. Schreiber, K. N. Cassemiro, V. Potoček, A. Gábris, I. Jex, and C. Silberhorn, *Physical Review Letters* **106**, 180403 (2011).
- [24] A. Schreiber, A. Gabris, P. P. Rohde, K. Laiho, M. Stefanak, V. Potocek, C. Hamilton, I. Jex, and C. Silberhorn, *Science* **336**, 55 (2012).
- [25] T. Nitsche, F. Elster, J. Novotný, A. Gábris, I. Jex, S. Barkhofen, and C. Silberhorn, *New Journal of Physics* **18**, 063017 (2016).
- [26] S. Barkhofen, T. Nitsche, F. Elster, L. Lorz, A. Gábris, I. Jex, and C. Silberhorn, *Physical Review A* **96**, 033846 (2017).
- [27] C. Chen, X. Ding, J. Qin, Y. He, Y.-H. Luo, M.-C. Chen, C. Liu, X.-L. Wang, W.-J. Zhang, H. Li, L.-X. You, Z. Wang, D.-W. Wang, B. C. Sanders, C.-Y. Lu, and J.-W. Pan, *Physical Review Letters* **121**, 100502 (2018).
- [28] T. Kitagawa, M. S. Rudner, E. Berg, and E. Demler, *Physical Review A* **82**, 033429 (2010).
- [29] T. Kitagawa, E. Berg, M. Rudner, and E. Demler, *Physical Review B* **82**, 235114 (2010).
- [30] T. Kitagawa, M. A. Broome, A. Fedrizzi, M. S. Rudner, E. Berg, I. Kassal, A. Aspuru-Guzik, E. Demler, and A. G. White, *Nature Communications* **3**, 882 (2012).
- [31] T. Kitagawa, *Quantum Information Processing* **11**, 1107 (2012).
- [32] K. v. Klitzing, G. Dorda, and M. Pepper, *Physical Review Letters* **45**, 494 (1980).
- [33] F. D. M. Haldane, *Physical Review Letters* **61**, 2015 (1988).
- [34] M. König, S. Wiedmann, C. Brune, A. Roth, H. Buhmann, L. W. Molenkamp, X.-L. Qi, and S.-C. Zhang, *Science* **318**, 766 (2007).
- [35] . Yalcnkaya and Z. Gedik, *Physical Review A* **92**, 042324 (2015).
- [36] See Supplemental Material.
- [37] H. Chalabi and E. Waks, *Physical Review A* **98**, 063832 (2018).
- [38] H. Pichler and P. Zoller, *Physical Review Letters* **116**, 093601 (2016).

Supplementary Information: A synthetic gauge field for two-dimensional time-multiplexed quantum random walks

In this supplementary material, we first explain the experimental details in the first section. The details of the theoretical analysis are summarized in the subsequent section.

I. EXPERIMENTAL DETAILS:

For the purpose of pulse generation in this random walk experiment, we have used a laser diode operating at the C-band of the telecom wavelength (1550nm). By modulation of this laser made by Bookham technology (LC25W5172BA-J34), we have generated pulses with the power of $10mW$ and the pulse duration of two nanoseconds. These pulses are sent into the setup with the repetition rate of $10\mu s$. We have used these pulses to initiate the random walk in our synthetic two dimensional space. Moreover, the polarization of the incident pulse is controlled using the polarization beam splitter.

Figure 1b in the manuscript shows the experimental setup used for making the synthetic two dimensional space. The initial pulse after passing through the first 50/50 beam splitter chooses to continue its path through either the 1m or 2m fiber length. This leads to different delays that can be regarded as choosing left or right direction in the x movement. By reaching the next beam splitter, the pulse chooses either the 130m or 100m fiber pool. This determines whether the pulse has gone to the up or down direction in the y movement. By this way, we encode the x and y movement of the pulses based on the delay in reaching the detectors. We have used 90/10 beam splitters to out-couple 10% of the light for the detection purposes.

In order to compensate the loss in the experimental setup, we have used semiconductor optical amplifiers made by Thorlabs (SOA1117S). These amplifiers, which are turned on for a fraction a repetition period at each cycle, provide the capability to amplify the pulses without ruining their phase coherence. However, in addition to amplifying the signal they increase the background noise due to spontaneous emission. Such noises should be filtered out using band-pass filter. For this purpose, we have used narrow band-pass filters ($< 0.3nm$) right after semiconductor optical amplifiers as shown in Fig. 1b.

Despite this compensation, the ratio of the optical pulse power at different positions of the synthetic space relative to the noise degrades with increasing time steps due to the diffusion and the added noise. Because of the degradation of the signal to noise ratio and the finite ratio of the time delays corresponding to x and y movements, we limited our measurement of the random walk distribution to 10 steps. By measuring the power of the pulses present in each step, we can determine the distribution of the random walk at every time step.

In addition, the polarization of the incident pulse varies by passing through the fiber network. To compensate these polarization changes, we have used polarization controllers in our setup.

Furthermore, we have used two phase modulators in this setup that apply opposite phases to the left and right moving pulses. These phase modulators (MPZ-LN-10-P-P-FA-FA) made by Cybel company can provide switching speed of $12Gb/s$ and have $3dB$ loss.

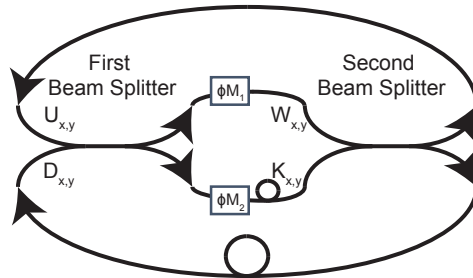


Figure S1. Simplified version of the schematic of the 2D random walk setup.

II. THEORETICAL ANALYSIS:

In the followings, the evolution of pulses (representing the random walkers) in the two-dimensional (2D) random walk is analyzed. For the theoretical analysis of the random walk, we can assume that all the losses in the setup including the losses caused by 90/10 beam splitters as well as phase modulators are fully compensated by the amplifiers. Moreover, we can assume that polarization controllers compensate all the polarization changes in the setup. Therefore, for theoretical analysis we can simplify the schematic and consider an ideal setup as shown in Fig. S1.

Two pulses just before the first beam splitter, $\begin{bmatrix} U_{x,y}^{(n)} \\ D_{x,y}^{(n)} \end{bmatrix}$, will produce the output pulses as (movement in x direction):

$$\begin{bmatrix} W_{x-1,y} \\ K_{x+1,y} \end{bmatrix} = \frac{1}{\sqrt{2}} \begin{bmatrix} e^{i\phi_{n,y}} & 0 \\ 0 & e^{-i\phi_{n,y}} \end{bmatrix} \begin{bmatrix} 1 & -1 \\ 1 & 1 \end{bmatrix} \begin{bmatrix} U_{x,y}^{(n)} \\ D_{x,y}^{(n)} \end{bmatrix}.$$

Note that the applied phases are assumed to be explicit functions of time step (n) as well as y coordinate but not x coordinate due to experimental limitations.

Pulses which are input to the second beam splitter, $\begin{bmatrix} W_{x,y} \\ K_{x,y} \end{bmatrix}$, will produce the outputs as (movement in y direction):

$$\begin{bmatrix} U_{x,y+1}^{(n+1)} \\ D_{x,y-1}^{(n+1)} \end{bmatrix} = \frac{1}{\sqrt{2}} \begin{bmatrix} 1 & -1 \\ 1 & 1 \end{bmatrix} \begin{bmatrix} W_{x,y} \\ K_{x,y} \end{bmatrix}$$

By considering the pulse of $\begin{bmatrix} W_{x-1,y} \\ 0 \end{bmatrix}$ caused by $\begin{bmatrix} U_{x,y}^{(n)} \\ D_{x,y}^{(n)} \end{bmatrix}$, we have:

$$\begin{aligned} \begin{bmatrix} U_{x-1,y+1}^{(n+1)} \\ D_{x-1,y-1}^{(n+1)} \end{bmatrix} &= \frac{1}{\sqrt{2}} \begin{bmatrix} 1 & -1 \\ 1 & 1 \end{bmatrix} \begin{bmatrix} W_{x-1,y} \\ 0 \end{bmatrix} \\ &= \frac{1}{2} \begin{bmatrix} 1 & -1 \\ 1 & 1 \end{bmatrix} \begin{bmatrix} 1 & 0 \\ 0 & 0 \end{bmatrix} \begin{bmatrix} e^{i\phi_{n,y}} & 0 \\ 0 & e^{-i\phi_{n,y}} \end{bmatrix} \begin{bmatrix} 1 & -1 \\ 1 & 1 \end{bmatrix} \begin{bmatrix} U_{x,y}^{(n)} \\ D_{x,y}^{(n)} \end{bmatrix} \\ &= \frac{1}{2} \begin{bmatrix} e^{i\phi_{n,y}} & -e^{i\phi_{n,y}} \\ e^{i\phi_{n,y}} & -e^{i\phi_{n,y}} \end{bmatrix} \begin{bmatrix} U_{x,y}^{(n)} \\ D_{x,y}^{(n)} \end{bmatrix} \end{aligned}$$

Furthermore, by considering the pulse of $\begin{bmatrix} 0 \\ K_{x+1,y} \end{bmatrix}$ caused by $\begin{bmatrix} U_{x,y}^{(n)} \\ D_{x,y}^{(n)} \end{bmatrix}$, we have:

$$\begin{aligned} \begin{bmatrix} U_{x+1,y+1}^{(n+1)} \\ D_{x+1,y-1}^{(n+1)} \end{bmatrix} &= \frac{1}{\sqrt{2}} \begin{bmatrix} 1 & -1 \\ 1 & 1 \end{bmatrix} \begin{bmatrix} 0 \\ K_{x+1,y} \end{bmatrix} \\ &= \frac{1}{2} \begin{bmatrix} 1 & -1 \\ 1 & 1 \end{bmatrix} \begin{bmatrix} 0 & 0 \\ 0 & 1 \end{bmatrix} \begin{bmatrix} e^{i\phi_{n,y}} & 0 \\ 0 & e^{-i\phi_{n,y}} \end{bmatrix} \begin{bmatrix} 1 & -1 \\ 1 & 1 \end{bmatrix} \begin{bmatrix} U_{x,y}^{(n)} \\ D_{x,y}^{(n)} \end{bmatrix} \\ &= \frac{1}{2} \begin{bmatrix} -e^{-i\phi_{n,y}} & -e^{-i\phi_{n,y}} \\ e^{-i\phi_{n,y}} & e^{-i\phi_{n,y}} \end{bmatrix} \begin{bmatrix} U_{x,y}^{(n)} \\ D_{x,y}^{(n)} \end{bmatrix} \end{aligned}$$

Therefore, $\begin{bmatrix} U_{x,y}^{(n)} \\ D_{x,y}^{(n)} \end{bmatrix}$ will produce the following pulses after traversing both of the beam splitters:

$$U_{x-1,y+1}^{(n+1)} = \frac{1}{2} \left(e^{i\phi_{n,y}} U_{x,y}^{(n)} - e^{i\phi_{n,y}} D_{x,y}^{(n)} \right)$$

$$U_{x+1,y+1}^{(n+1)} = \frac{1}{2} \left(-e^{-i\phi_{n,y}} U_{x,y}^{(n)} - e^{-i\phi_{n,y}} D_{x,y}^{(n)} \right)$$

$$D_{x-1,y-1}^{(n+1)} = \frac{1}{2} \left(e^{i\phi_{n,y}} U_{x,y}^{(n)} - e^{i\phi_{n,y}} D_{x,y}^{(n)} \right)$$

$$D_{x+1,y-1}^{(n+1)} = \frac{1}{2} \left(e^{-i\phi_{n,y}} U_{x,y}^{(n)} + e^{-i\phi_{n,y}} D_{x,y}^{(n)} \right)$$

Alternatively, based on the above results $\begin{bmatrix} U_{x,y}^{(n+1)} \\ D_{x,y}^{(n+1)} \end{bmatrix}$ can be produced from other pulses as:

$$U_{x,y}^{(n+1)} = \frac{e^{i\phi_{n,y-1}}}{2} \left(U_{x+1,y-1}^{(n)} - D_{x+1,y-1}^{(n)} \right) - \frac{e^{-i\phi_{n,y-1}}}{2} \left(U_{x-1,y-1}^{(n)} + D_{x-1,y-1}^{(n)} \right)$$

$$D_{x,y}^{(n+1)} = \frac{e^{i\phi_{n,y+1}}}{2} \left(U_{x+1,y+1}^{(n)} - D_{x+1,y+1}^{(n)} \right) + \frac{e^{-i\phi_{n,y+1}}}{2} \left(U_{x-1,y+1}^{(n)} + D_{x-1,y+1}^{(n)} \right)$$

The above two equations fully describe the evolution of pulses by time. We can prove that any constant phase independent of time and coordinate will not change the dynamics of evolution. For this purpose, we separate out any such constant phase from $\phi_{n,y}$ and we assume that $\phi_{n,y}$ can be written as:

$$\phi_{n,y} = \Phi + \phi'_{n,y}$$

Therefore:

$$U_{x,y}^{(n+1)} = \frac{e^{i\Phi+i\phi'_{n,y-1}}}{2} \left(U_{x+1,y-1}^{(n)} - D_{x+1,y-1}^{(n)} \right) - \frac{e^{-i\Phi-i\phi'_{n,y-1}}}{2} \left(U_{x-1,y-1}^{(n)} + D_{x-1,y-1}^{(n)} \right)$$

$$D_{x,y}^{(n+1)} = \frac{e^{i\Phi+i\phi'_{n,y+1}}}{2} \left(U_{x+1,y+1}^{(n)} - D_{x+1,y+1}^{(n)} \right) + \frac{e^{-i\Phi-i\phi'_{n,y+1}}}{2} \left(U_{x-1,y+1}^{(n)} + D_{x-1,y+1}^{(n)} \right)$$

By defining U' and D' from U and D as:

$$U'_{x,y}{}^{(n)} = e^{ix\Phi} U_{x,y}^{(n)}$$

$$D'_{x,y}{}^{(n)} = e^{ix\Phi} D_{x,y}^{(n)}$$

We have:

$$U'_{x,y}{}^{(n+1)} = \frac{e^{i\phi'_{n,y-1}}}{2} \left(U'_{x+1,y-1}{}^{(n)} - D'_{x+1,y-1}{}^{(n)} \right) - \frac{e^{-i\phi'_{n,y-1}}}{2} \left(U'_{x-1,y-1}{}^{(n)} + D'_{x-1,y-1}{}^{(n)} \right)$$

$$D'_{x,y}{}^{(n+1)} = \frac{e^{i\phi'_{n,y+1}}}{2} \left(U'_{x+1,y+1}{}^{(n)} - D'_{x+1,y+1}{}^{(n)} \right) + \frac{e^{-i\phi'_{n,y+1}}}{2} \left(U'_{x-1,y+1}{}^{(n)} + D'_{x-1,y+1}{}^{(n)} \right)$$

This shows that the evolution is invariant under such a constant phase application.

By defining $S_{x,y}^{(n)} = U_{x,y}^{(n)} + D_{x,y}^{(n)}$ and $P_{x,y}^{(n)} = U_{x,y}^{(n)} - D_{x,y}^{(n)}$, the obtained equations can be written as:

$$\begin{bmatrix} S_{x,y}^{(n+1)} \\ P_{x,y}^{(n+1)} \end{bmatrix} = \frac{1}{2} \begin{bmatrix} e^{-i\phi_{n,y+1}} & e^{i\phi_{n,y+1}} & -e^{-i\phi_{n,y-1}} & e^{i\phi_{n,y-1}} \\ -e^{-i\phi_{n,y+1}} & -e^{i\phi_{n,y+1}} & -e^{-i\phi_{n,y-1}} & e^{i\phi_{n,y-1}} \end{bmatrix} \begin{bmatrix} S_{x-1,y+1}^{(n)} \\ P_{x+1,y+1}^{(n)} \\ S_{x-1,y-1}^{(n)} \\ P_{x+1,y-1}^{(n)} \end{bmatrix}$$

Now that we have the governing equation in the real space, we can think about its solution in the Fourier space. By defining $s_{k_x, k_y}^{(n)}$ and $p_{k_x, k_y}^{(n)}$ as Fourier transforms of $S_{x,y}^{(n)}$ and $P_{x,y}^{(n)}$, we have:

$$\begin{bmatrix} S_{x,y}^{(n)} \\ P_{x,y}^{(n)} \end{bmatrix} = \frac{1}{4\pi^2} \begin{bmatrix} \int \int_{k_x, k_y} s_{k_x, k_y}^{(n)} e^{ik_x x + ik_y y} dk_x dk_y \\ \int \int_{k_x, k_y} p_{k_x, k_y}^{(n)} e^{ik_x x + ik_y y} dk_x dk_y \end{bmatrix}$$

Therefore:

$$\begin{bmatrix} \int \int_{k_x, k_y} s_{k_x, k_y}^{(n+1)} e^{ik_x x + ik_y y} dk_x dk_y \\ \int \int_{k_x, k_y} p_{k_x, k_y}^{(n+1)} e^{ik_x x + ik_y y} dk_x dk_y \end{bmatrix} = \frac{1}{2} \begin{bmatrix} e^{-i\phi_{n,y+1}} & e^{i\phi_{n,y+1}} & -e^{-i\phi_{n,y-1}} & e^{i\phi_{n,y-1}} \\ -e^{-i\phi_{n,y+1}} & -e^{i\phi_{n,y+1}} & -e^{-i\phi_{n,y-1}} & e^{i\phi_{n,y-1}} \end{bmatrix} \times \begin{bmatrix} \int \int_{k_x, k_y} e^{ik_y - ik_x} s_{k_x, k_y}^{(n)} e^{ik_x x + ik_y y} dk_x dk_y \\ \int \int_{k_x, k_y} e^{ik_x + ik_y} p_{k_x, k_y}^{(n)} e^{ik_x x + ik_y y} dk_x dk_y \\ \int \int_{k_x, k_y} e^{-ik_x - ik_y} s_{k_x, k_y}^{(n)} e^{ik_x x + ik_y y} dk_x dk_y \\ \int \int_{k_x, k_y} e^{ik_x - ik_y} p_{k_x, k_y}^{(n)} e^{ik_x x + ik_y y} dk_x dk_y \end{bmatrix}$$

This equation can be used to solve the Fourier transforms as functions of the time step. In the following subsections, we solve this equation for two cases of no phase modulation as well as time independent linear phase modulation.

A. Zero phase modulation:

For the case of no applied phase, we have:

$$\begin{bmatrix} s_{k_x, k_y}^{(n+1)} \\ p_{k_x, k_y}^{(n+1)} \end{bmatrix} = \begin{bmatrix} ie^{-ik_x} \sin(k_y) & e^{ik_x} \cos(k_y) \\ -e^{-ik_x} \cos(k_y) & -ie^{ik_x} \sin(k_y) \end{bmatrix} \begin{bmatrix} s_{k_x, k_y}^{(n)} \\ p_{k_x, k_y}^{(n)} \end{bmatrix}$$

Note that the evolution matrix has the determinant of 1. Based on this matrix, the effective Hamiltonian, $H_{eff} = i \log(U)$, is given by:

$$H = \begin{pmatrix} -\cos(k_x) \sin(k_y) & ie^{ik_x} \cos(k_y) \\ -ie^{-ik_x} \cos(k_y) & \cos(k_x) \sin(k_y) \end{pmatrix} \frac{\arccos(\sin(k_x) \sin(k_y))}{\sin(\arccos(\sin(k_x) \sin(k_y)))}$$

The obtained Hamiltonian is obviously hermitian. The eigenvalues of this Hamiltonian are given by:

$$E_{\pm} = \pm \arccos(\sin(k_x) \sin(k_y))$$

Moreover, the eigenvectors are given by:

$$\begin{pmatrix} \cos(k_x) \sin(k_y) \mp \sqrt{1 - \sin^2(k_x) \sin^2(k_y)} \\ ie^{-ik_x} \cos(k_y) \end{pmatrix}$$

Therefore, by defining S as

$$S = \begin{pmatrix} \cos(k_x) \sin(k_y) - \sqrt{1 - \sin^2(k_x) \sin^2(k_y)} & \cos(k_x) \sin(k_y) + \sqrt{1 - \sin^2(k_x) \sin^2(k_y)} \\ ie^{-ik_x} \cos(k_y) & ie^{-ik_x} \cos(k_y) \end{pmatrix},$$

we can write the Hamiltonian as:

$$H = S \begin{pmatrix} E_+ & 0 \\ 0 & E_- \end{pmatrix} S^{-1}$$

Based on the obtained eigen-energies, the band diagram for the zero phase modulation has been plotted in Fig. 3a. The evolution after n steps is given by:

$$\begin{aligned} \begin{bmatrix} s_{k_x, k_y}^{(n)} \\ p_{k_x, k_y}^{(n)} \end{bmatrix} &= \begin{bmatrix} ie^{-ik_x} \sin(k_y) & e^{ik_x} \cos(k_y) \\ -e^{-ik_x} \cos(k_y) & -ie^{ik_x} \sin(k_y) \end{bmatrix}^n \begin{bmatrix} s_{k_x, k_y}^{(0)} \\ p_{k_x, k_y}^{(0)} \end{bmatrix} \\ &= U^n \begin{bmatrix} s_{k_x, k_y}^{(0)} \\ p_{k_x, k_y}^{(0)} \end{bmatrix} \end{aligned}$$

The deterministic equation for the evolution matrix, $\lambda^2 - 2\lambda \sin(k_y) \sin(k_x) + 1 = 0$, gives the following Eigenvalues:

$$\lambda_{1,2} = \sin(k_y) \sin(k_x) \mp \sqrt{\sin^2(k_y) \sin^2(k_x) - 1}$$

They are equal to $e^{-iE_{\pm}}$ as we expect. We can define the following two orthogonal functions for performing the matrix power:

$$e_{k_x, k_y}^{(n)}, f_{k_x, k_y}^{(n)} = e^{-ik_x} \cos(k_y) s_{k_x, k_y}^{(n)} + \left(i \cos(k_x) \sin(k_y) \pm \sqrt{\sin^2(k_y) \sin^2(k_x) - 1} \right) p_{k_x, k_y}^{(n)}$$

These functions obey the following independent equations:

$$\begin{aligned} e_{k_x, k_y}^{(n+1)} &= \left(\sin(k_x) \sin(k_y) - \sqrt{\sin^2(k_y) \sin^2(k_x) - 1} \right) e_{k_x, k_y}^{(n)} \\ f_{k_x, k_y}^{(n+1)} &= \left(\sin(k_x) \sin(k_y) + \sqrt{\sin^2(k_y) \sin^2(k_x) - 1} \right) f_{k_x, k_y}^{(n)} \end{aligned}$$

Assuming that the whole evolution is caused by a single pulse at the origin ($U_{x,y}^{(0)} = \delta(x) \delta(y)$, $D_{x,y}^{(0)} = 0$ which is equivalent to $S_{x,y}^{(0)} = \delta(x) \delta(y)$, $P_{x,y}^{(0)} = \delta(x) \delta(y)$), then we would have (the Fourier transform of Dirac delta function is constant unity):

$$\begin{bmatrix} s_{k_x, k_y}^{(0)} \\ p_{k_x, k_y}^{(0)} \end{bmatrix} = \begin{bmatrix} 1 \\ 1 \end{bmatrix}$$

Therefore, for the down channel pulses, $d_{k_x, k_y}^{(n)} = 0.5 (s_{k_x, k_y}^{(n)} - p_{k_x, k_y}^{(n)})$, we have:

$$\begin{aligned} d_{k_x, k_y}^{(n)} &= 0.5 (s_{k_x, k_y}^{(n)} - p_{k_x, k_y}^{(n)}) \\ &= e^{ik_y} \cos(k_x) \frac{\sin(n \arccos(\sin(k_x) \sin(k_y)))}{\sin(\arccos(\sin(k_x) \sin(k_y)))} \end{aligned}$$

All the moments such as distribution variances and averages ($\langle x^2 \rangle_D$, $\langle y^2 \rangle_D$, $\langle x \rangle_D$ and $\langle y \rangle_D$) as functions of time step n , can be obtained from the above expression.

Based on the fact that:

$$d_{k_x, k_y}^{(n)} = \sum_{x,y} D_{x,y}^{(n)} e^{-ik_x x} e^{-ik_y y}$$

Then:

$$d_{l_x, l_y}^{(n)*} d_{k_x, k_y}^{(n)} = \sum_{p,q} \sum_{x,y} e^{-i(k_x x - l_x p)} e^{-i(k_y y - l_y q)} D_{p,q}^{(n)*} D_{x,y}^{(n)}$$

Therefore, the following equations can be obtained, straightforwardly:

$$\begin{aligned} P_D &= \sum_{x,y} |D_{x,y}^{(n)}|^2 = \frac{1}{4\pi^2} \int_{k_y=0}^{2\pi} \int_{k_x=0}^{2\pi} |d_{k_x, k_y}^{(n)}|^2 dk_x dk_y \\ &= \frac{1}{4\pi^2} \int_{k_y=0}^{2\pi} \int_{k_x=0}^{2\pi} \cos^2(k_x) \frac{\sin^2(n \arccos(\sin(k_x) \sin(k_y)))}{\sin^2(\arccos(\sin(k_x) \sin(k_y)))} dk_x dk_y \end{aligned}$$

$$\langle x \rangle_D = \sum_{x,y} x |D_{x,y}^{(n)}|^2 = \frac{1}{4\pi^2} \int_{k_y=0}^{2\pi} \int_{k_x=0}^{2\pi} d_{k_x, k_y}^{(n)*} \left(i \frac{d}{dk_x} \right) d_{k_x, k_y}^{(n)} dk_x dk_y = 0$$

$$\begin{aligned} \langle y \rangle_D &= \sum_{x,y} y |D_{x,y}^{(n)}|^2 = \frac{1}{4\pi^2} \int_{k_y=0}^{2\pi} \int_{k_x=0}^{2\pi} d_{k_x, k_y}^{(n)*} \left(i \frac{d}{dk_y} \right) d_{k_x, k_y}^{(n)} dk_x dk_y \\ &= \frac{-1}{4\pi^2} \int_{k_y=0}^{2\pi} \int_{k_x=0}^{2\pi} \cos^2(k_x) \frac{\sin^2(n \arccos(\sin(k_x) \sin(k_y)))}{\sin^2(\arccos(\sin(k_x) \sin(k_y)))} dk_x dk_y = -P_D \end{aligned}$$

$$\begin{aligned}
\langle x^2 \rangle_D &= \sum_{x,y} x^2 |D_{x,y}^{(n)}|^2 = \frac{1}{4\pi^2} \int_{k_y=0}^{2\pi} \int_{k_x=0}^{2\pi} d_{k_x,k_y}^{(n)*} \left(i \frac{d}{dk_x} \right)^2 d_{k_x,k_y}^{(n)} dk_x dk_y \\
&= \frac{n^2}{4\pi^2} \int_{k_y=0}^{2\pi} \int_{k_x=0}^{2\pi} \frac{\cos^4(k_x) \sin^2(k_y)}{(1 - \sin^2(k_x) \sin^2(k_y))^2} \sin^2(n \cos^{-1}(\sin(k_x) \sin(k_y))) dk_x dk_y \\
&\quad - \frac{3n}{8\pi^2} \int_{k_y=0}^{2\pi} \int_{k_x=0}^{2\pi} \frac{\sin(k_x) \sin(k_y) \cos^2(k_x) \cos^2(k_y)}{(1 - \sin^2(k_x) \sin^2(k_y))^{5/2}} \sin(2n \cos^{-1}(\sin(k_x) \sin(k_y))) dk_x dk_y \\
&\quad + \frac{3}{4\pi^2} \int_{k_y=0}^{2\pi} \int_{k_x=0}^{2\pi} \frac{\sin^2(k_x) \sin^2(k_y) \cos^2(k_x) \cos^2(k_y)}{(1 - \sin^2(k_x) \sin^2(k_y))^3} \sin^2(n \cos^{-1}(\sin(k_x) \sin(k_y))) dk_x dk_y \\
&\quad + \frac{1}{4\pi^2} \int_{k_y=0}^{2\pi} \int_{k_x=0}^{2\pi} \frac{\cos^2(k_x) \cos^2(k_y)}{(1 - \sin^2(k_x) \sin^2(k_y))^2} \sin^2(n \cos^{-1}(\sin(k_x) \sin(k_y))) dk_x dk_y
\end{aligned}$$

$$\begin{aligned}
\langle y^2 \rangle_D &= \sum_{x,y} y^2 |D_{x,y}^{(n)}|^2 = \frac{1}{4\pi^2} \int_{k_y=0}^{2\pi} \int_{k_x=0}^{2\pi} d_{k_x,k_y}^{(n)*} \left(i \frac{d}{dk_y} \right)^2 d_{k_x,k_y}^{(n)} dk_x dk_y \\
&= \frac{n^2}{4\pi^2} \int_{k_y=0}^{2\pi} \int_{k_x=0}^{2\pi} \frac{\sin^2(k_x) \cos^2(k_x) \cos^2(k_y)}{(1 - \sin^2(k_x) \sin^2(k_y))^2} \sin^2(n \cos^{-1}(\sin(k_x) \sin(k_y))) dk_x dk_y \\
&\quad + \frac{n}{4\pi^2} \int_{k_y=0}^{2\pi} \int_{k_x=0}^{2\pi} \frac{\cos^2(k_x) \sin(k_x) \sin(k_y)}{(1 - \sin^2(k_x) \sin^2(k_y))^{3/2}} \sin(2n \cos^{-1}(\sin(k_x) \sin(k_y))) dk_x dk_y \\
&\quad - \frac{3n}{8\pi^2} \int_{k_y=0}^{2\pi} \int_{k_x=0}^{2\pi} \frac{\cos^4(k_x) \sin(k_x) \sin(k_y)}{(1 - \sin^2(k_x) \sin^2(k_y))^{5/2}} \sin(2n \cos^{-1}(\sin(k_x) \sin(k_y))) dk_x dk_y \\
&\quad + \frac{1}{2\pi^2} \int_{k_y=0}^{2\pi} \int_{k_x=0}^{2\pi} \frac{\cos^2(k_x) (\sin^2(k_x) \cos^2(k_y) - 1)}{(1 - \sin^2(k_x) \sin^2(k_y))^2} \sin^2(n \cos^{-1}(\sin(k_x) \sin(k_y))) dk_x dk_y \\
&\quad + \frac{3}{4\pi^2} \int_{k_y=0}^{2\pi} \int_{k_x=0}^{2\pi} \frac{\cos^4(k_x)}{(1 - \sin^2(k_x) \sin^2(k_y))^3} \sin^2(n \cos^{-1}(\sin(k_x) \sin(k_y))) dk_x dk_y
\end{aligned}$$

In the limit of large n , we have:

$$P_D \rightarrow \frac{1}{8\pi^2} \int_{k_y=0}^{2\pi} \int_{k_x=0}^{2\pi} \frac{\cos^2(k_x)}{\sin^2(\arccos(\sin(k_x) \sin(k_y)))} dk_x dk_y = \frac{1}{\pi}$$

$$\langle x \rangle_D \rightarrow 0$$

$$\langle y \rangle_D \rightarrow -\frac{1}{\pi}$$

$$\langle x^2 \rangle_D \rightarrow \frac{n^2}{8\pi^2} \int_{k_y=0}^{2\pi} \int_{k_x=0}^{2\pi} \frac{\cos^4(k_x) \sin^2(k_y)}{(1 - \sin^2(k_x) \sin^2(k_y))^2} dk_x dk_y = \frac{n^2}{2\pi}$$

$$\langle y^2 \rangle_D \rightarrow \frac{n^2}{8\pi^2} \int_{k_y=0}^{2\pi} \int_{k_x=0}^{2\pi} \frac{\sin^2(k_x) \cos^2(k_x) \cos^2(k_y)}{(1 - \sin^2(k_x) \sin^2(k_y))^2} dk_x dk_y = \frac{n^2}{6\pi}$$

which shows that $\langle y^2 \rangle_D$ is three times less than $\langle x^2 \rangle_D$. These results prove that the spatial quadratic means of the random walk distribution linearly vary with the time step. Note that these average values are normalized relative to

the total power in the up and down channels. However, they can also be normalized relative to the total power present in the corresponding channel. Such a normalization has been used in the manuscript to calculate the experimental and theoretical quadratic means. Since the probabilities of P_D and P_U tend toward constant values, by the latter normalization the asymptotic behavior of the quadratic means remains linear relative to the time step.

It is interesting to test some first steps:

$$d_{k_x, k_y}^{(0)} = 0 \rightarrow D_{x,y}^{(0)} = 0$$

$$d_{k_x, k_y}^{(1)} = e^{ik_y} \cos(k_x) \rightarrow D_{x,y}^{(1)} = \begin{cases} 0.5 (x = -1, y = -1) \\ 0.5 (x = 1, y = -1) \\ 0 (Otherwise) \end{cases}$$

$$d_{k_x, k_y}^{(2)} = e^{ik_y} \sin(2k_x) \sin(k_y) \rightarrow D_{x,y}^{(2)} = \begin{cases} -0.25 (x = -2, y = -2) \\ 0 (x = 0, y = -2) \\ 0.25 (x = 2, y = -2) \\ 0.25 (x = -2, y = 0) \\ 0 (x = 0, y = 0) \\ -0.25 (x = 2, y = 0) \\ 0 (Otherwise) \end{cases}$$

$$d_{k_x, k_y}^{(3)} = e^{ik_y} \cos(k_x) (\cos(2k_x) \cos(2k_y) - \cos(2k_x) - \cos(2k_y)) \rightarrow D_{x,y}^{(3)} = \begin{cases} 0.125 (x = -3, y = -3) \\ -0.125 (x = -1, y = -3) \\ -0.125 (x = 1, y = -3) \\ 0.125 (x = 3, y = -3) \\ -0.25 (x = -3, y = -1) \\ -0.25 (x = -1, y = -1) \\ -0.25 (x = 1, y = -1) \\ -0.25 (x = 3, y = -1) \\ 0.125 (x = -3, y = 1) \\ -0.125 (x = -1, y = 1) \\ -0.125 (x = 1, y = 1) \\ 0.125 (x = 3, y = 1) \\ 0 (Otherwise) \end{cases}$$

Similarly, we can investigate the up channel:

$$u_{k_x, k_y}^{(n)} = 0.5 \left(s_{k_x, k_y}^{(n)} + p_{k_x, k_y}^{(n)} \right)$$

$$= \cos(n \arccos(\sin(k_x) \sin(k_y))) + i \cos(k_y) \sin(k_x) \frac{\sin(n \arccos(\sin(k_x) \sin(k_y)))}{\sin(\arccos(\sin(k_x) \sin(k_y)))}$$

$$P_U = \sum_{x,y} \left| U_{x,y}^{(n)} \right|^2 = \frac{1}{4\pi^2} \int_{k_y=0}^{2\pi} \int_{k_x=0}^{2\pi} \left| u_{k_x, k_y}^{(n)} \right|^2 dk_x dk_y$$

$$= \frac{1}{4\pi^2} \int_{k_y=0}^{2\pi} \int_{k_x=0}^{2\pi} \cos^2(n \arccos(\sin(k_x) \sin(k_y))) dk_x dk_y$$

$$+ \frac{1}{4\pi^2} \int_{k_y=0}^{2\pi} \int_{k_x=0}^{2\pi} \cos^2(k_y) \sin^2(k_x) \frac{\sin^2(n \arccos(\sin(k_x) \sin(k_y)))}{\sin^2(\arccos(\sin(k_x) \sin(k_y)))} dk_x dk_y$$

$$\langle x \rangle_U = \sum_{x,y} x \left| U_{x,y}^{(n)} \right|^2 = \frac{1}{4\pi^2} \int_{k_y=0}^{2\pi} \int_{k_x=0}^{2\pi} u_{k_x, k_y}^{(n)*} \left(i \frac{d}{dk_x} \right) u_{k_x, k_y}^{(n)} dk_x dk_y = 0$$

$$\begin{aligned}
\langle y \rangle_U &= \sum_{x,y} y |U_{x,y}^{(n)}|^2 = \frac{1}{4\pi^2} \int_{k_y=0}^{2\pi} \int_{k_x=0}^{2\pi} u_{k_x,k_y}^{(n)*} \left(i \frac{d}{dk_y} \right) u_{k_x,k_y}^{(n)} dk_x dk_y \\
&= \left(1 - \frac{2}{\pi} \right) n + \frac{1}{8\pi^2} \int_{k_y=0}^{2\pi} \int_{k_x=0}^{2\pi} \frac{\cos^2(k_x) \sin(k_x) \sin(k_y)}{(1 - \sin^2(k_x) \sin^2(k_y))^{3/2}} \sin(2n \arccos(\sin(k_x) \sin(k_y))) dk_x dk_y
\end{aligned}$$

$$\begin{aligned}
\langle x^2 \rangle_U &= \sum_{x,y} x^2 |U_{x,y}^{(n)}|^2 = \frac{1}{4\pi^2} \int_{k_y=0}^{2\pi} \int_{k_x=0}^{2\pi} u_{k_x,k_y}^{(n)*} \left(i \frac{d}{dk_x} \right)^2 u_{k_x,k_y}^{(n)} dk_x dk_y \\
&= \frac{n^2}{8\pi^2} \int_{k_y=0}^{2\pi} \int_{k_x=0}^{2\pi} \frac{\cos^2(k_x) \sin^2(k_y) (1 + \sin^2(k_x) \cos(2k_y))}{(1 - \sin^2(k_x) \sin^2(k_y))^2} dk_x dk_y \\
&+ \frac{n^2}{8\pi^2} \int_{k_y=0}^{2\pi} \int_{k_x=0}^{2\pi} \frac{\cos^4(k_x) \sin^2(k_y)}{(1 - \sin^2(k_x) \sin^2(k_y))^2} \cos(2n \arccos(\sin(k_x) \sin(k_y))) dk_x dk_y \\
&+ \frac{3n}{8\pi^2} \int_{k_y=0}^{2\pi} \int_{k_x=0}^{2\pi} \frac{\sin(k_x) \sin(k_y) \cos^2(k_x) \cos^2(k_y)}{(1 - \sin^2(k_x) \sin^2(k_y))^{5/2}} \sin(2n \arccos(\sin(k_x) \sin(k_y))) dk_x dk_y \\
&+ \frac{1}{4\pi^2} \int_{k_y=0}^{2\pi} \int_{k_x=0}^{2\pi} \frac{\sin^2(k_x) \cos^4(k_y)}{(1 - \sin^2(k_x) \sin^2(k_y))^3} \sin^2(n \arccos(\sin(k_x) \sin(k_y))) dk_x dk_y \\
&- \frac{1}{2\pi^2} \int_{k_y=0}^{2\pi} \int_{k_x=0}^{2\pi} \frac{\sin^2(k_x) \sin^2(k_y) \cos^2(k_x) \cos^2(k_y)}{(1 - \sin^2(k_x) \sin^2(k_y))^3} \sin^2(n \arccos(\sin(k_x) \sin(k_y))) dk_x dk_y
\end{aligned}$$

$$\begin{aligned}
\langle y^2 \rangle_U &= \sum_{x,y} y^2 |U_{x,y}^{(n)}|^2 = \frac{1}{4\pi^2} \int_{k_y=0}^{2\pi} \int_{k_x=0}^{2\pi} u_{k_x,k_y}^{(n)*} \left(i \frac{d}{dk_y} \right)^2 u_{k_x,k_y}^{(n)} dk_x dk_y \\
&= \frac{n^2}{8\pi^2} \int_{k_y=0}^{2\pi} \int_{k_x=0}^{2\pi} \frac{\sin^2(k_x) \cos^2(k_y) (1 + \sin^2(k_x) \cos(2k_y))}{(1 - \sin^2(k_x) \sin^2(k_y))^2} dk_x dk_y \\
&+ \frac{n^2}{8\pi^2} \int_{k_y=0}^{2\pi} \int_{k_x=0}^{2\pi} \frac{\sin^2(k_x) \cos^2(k_x) \cos^2(k_y)}{(1 - \sin^2(k_x) \sin^2(k_y))^2} \cos(2n \arccos(\sin(k_x) \sin(k_y))) dk_x dk_y \\
&+ \frac{3n}{8\pi^2} \int_{k_y=0}^{2\pi} \int_{k_x=0}^{2\pi} \frac{\cos^4(k_x) \sin(k_x) \sin(k_y)}{(1 - \sin^2(k_x) \sin^2(k_y))^{5/2}} \sin(2n \arccos(\sin(k_x) \sin(k_y))) dk_x dk_y \\
&- \frac{n}{4\pi^2} \int_{k_y=0}^{2\pi} \int_{k_x=0}^{2\pi} \frac{\cos^2(k_x) \sin(k_x) \sin(k_y)}{(1 - \sin^2(k_x) \sin^2(k_y))^{3/2}} \sin(2n \arccos(\sin(k_x) \sin(k_y))) dk_x dk_y \\
&+ \frac{3}{4\pi^2} \int_{k_y=0}^{2\pi} \int_{k_x=0}^{2\pi} \frac{\sin^2(k_x) \cos^2(k_x) \cos^2(k_y)}{(1 - \sin^2(k_x) \sin^2(k_y))^3} \sin^2(n \arccos(\sin(k_x) \sin(k_y))) dk_x dk_y \\
&- \frac{1}{2\pi^2} \int_{k_y=0}^{2\pi} \int_{k_x=0}^{2\pi} \frac{\sin^2(k_x) \cos^2(k_x) \cos^2(k_y)}{(1 - \sin^2(k_x) \sin^2(k_y))^2} \sin^2(n \arccos(\sin(k_x) \sin(k_y))) dk_x dk_y
\end{aligned}$$

In the limit of large n , we have:

$$P_U \rightarrow \frac{1}{2} + \frac{1}{8\pi^2} \int_{k_y=0}^{2\pi} \int_{k_x=0}^{2\pi} \frac{\cos^2(k_y) \sin^2(k_x)}{\sin^2(\arccos(\sin(k_x) \sin(k_y)))} dk_x dk_y = 1 - \frac{1}{\pi}$$

$$\langle x \rangle_U \rightarrow 0$$

$$\langle y \rangle_U \rightarrow \left(1 - \frac{2}{\pi}\right) n$$

$$\langle x^2 \rangle_U \rightarrow \frac{n^2}{8\pi^2} \int_{k_y=0}^{2\pi} \int_{k_x=0}^{2\pi} \frac{\cos^2(k_x) \sin^2(k_y) (1 + \sin^2(k_x) \cos(2k_y))}{(1 - \sin^2(k_x) \sin^2(k_y))^2} dk_x dk_y = \left(1 - \frac{5}{2\pi}\right) n^2$$

$$\langle y^2 \rangle_U \rightarrow \frac{n^2}{8\pi^2} \int_{k_y=0}^{2\pi} \int_{k_x=0}^{2\pi} \frac{\sin^2(k_x) \cos^2(k_y) (1 + \sin^2(k_x) \cos(2k_y))}{(1 - \sin^2(k_x) \sin^2(k_y))^2} dk_x dk_y = \left(1 - \frac{13}{6\pi}\right) n^2$$

For the first few steps, we have:

$$u_{k_x, k_y}^{(0)} = 1 \rightarrow U_{x,y}^{(0)} = \delta(x) \delta(y)$$

$$u_{k_x, k_y}^{(1)} = ie^{-ik_y} \sin(k_x) \rightarrow U_{x,y}^{(1)} = \begin{cases} 0.5 (x = -1, y = 1) \\ -0.5 (x = 1, y = 1) \\ 0 (Otherwise) \end{cases}$$

$$u_{k_x, k_y}^{(2)} = -e^{-ik_y} (\cos(k_y) + i \cos(2k_x) \sin(k_y)) \rightarrow U_{x,y}^{(2)} = \begin{cases} -0.25 (x = -2, y = 0) \\ -0.5 (x = 0, y = 0) \\ -0.25 (x = 2, y = 0) \\ 0.25 (x = -2, y = 2) \\ -0.5 (x = 0, y = 2) \\ 0.25 (x = 2, y = 2) \\ 0 (Otherwise) \end{cases}$$

$$u_{k_x, k_y}^{(3)} = ie^{-ik_y} \sin(k_x) (\cos(2k_x) \cos(2k_y) - 2 \cos^2(k_x) + i \sin(2k_y)) \rightarrow U_{x,y}^{(3)} = \begin{cases} 0.125 (x = -3, y = -1) \\ 0.125 (x = -1, y = -1) \\ -0.125 (x = 1, y = -1) \\ -0.125 (x = 3, y = -1) \\ -0.25 (x = -3, y = 1) \\ -0.25 (x = -1, y = 1) \\ 0.25 (x = 1, y = 1) \\ 0.25 (x = 3, y = 1) \\ 0.125 (x = -3, y = 3) \\ -0.375 (x = -1, y = 3) \\ 0.375 (x = 1, y = 3) \\ -0.125 (x = 3, y = 3) \\ 0 (Otherwise) \end{cases}$$

These are consistent with what we expect from recursive analysis of evolution.

B. Time independent phase modulation:

Uniform modulation:

For the case of time independent linear phase modulation, $\phi_{n,y} = y\phi$, we have:

$$\begin{bmatrix} s_{k_x, k_y}^{(n+1)} \\ p_{k_x, k_y}^{(n+1)} \end{bmatrix} = \begin{bmatrix} ie^{-ik_x} \sin(k_y) & e^{ik_x} \cos(k_y) \\ -e^{-ik_x} \cos(k_y) & -ie^{ik_x} \sin(k_y) \end{bmatrix} \begin{bmatrix} s_{k_x, k_y + \phi}^{(n)} \\ p_{k_x, k_y - \phi}^{(n)} \end{bmatrix}$$

For rational values of $\phi/2\pi = p/q$, we can consider $s_{k_x, k_y}, s_{k_x, k_y + \phi}, s_{k_x, k_y + 2\phi}, \dots, s_{k_x, k_y + (q-1)\phi}$ as well as $p_{k_x, k_y}, p_{k_x, k_y + \phi}, p_{k_x, k_y + 2\phi}, \dots, p_{k_x, k_y + (q-1)\phi}$ together as a vector. Then we can obtain the evolution equation for this vector. Note that this approach does not work for irrational values of $\phi/2\pi$. By representing this vector as

$$\psi^{(n)} = \left[s_{k_x, k_y}^{(n)} \quad s_{k_x, k_y + \phi}^{(n)} \quad \cdots \quad s_{k_x, k_y + (q-1)\phi}^{(n)} \quad p_{k_x, k_y}^{(n)} \quad p_{k_x, k_y + \phi}^{(n)} \quad \cdots \quad p_{k_x, k_y + (q-1)\phi}^{(n)} \right]^T,$$

we can write the evolution equation as:

$$\psi^{(n+1)} = M(k_x, k_y) \psi^{(n)}$$

In this equation, M is the evolution matrix and its size linearly increases by increasing q .

For a general propagation matrix, the eigen-energies can be calculated from the following characteristic equation:

$$|M - e^{iE} I| = 0$$

For instance, the evolution matrix for the case of $\phi = \pi$ is given by:

$$M = \begin{bmatrix} 0 & ie^{-ik_x} \sin(k_y) & 0 & e^{ik_x} \cos(k_y) \\ ie^{-ik_x} \sin(k_y + \pi) & 0 & e^{ik_x} \cos(k_y + \pi) & 0 \\ 0 & -e^{-ik_x} \cos(k_y) & 0 & -ie^{ik_x} \sin(k_y) \\ -e^{-ik_x} \cos(k_y + \pi) & 0 & -ie^{ik_x} \sin(k_y + \pi) & 0 \end{bmatrix}$$

In this case, the eigen-energies are given by:

$$E(k_x, k_y) = \pm \arccos \left(\pm \sqrt{1 - \sin^2(k_x) \sin^2(k_y)} \right)$$

Similar expressions can be obtained for other phase modulations. The obtained band diagrams for different values of ϕ are shown in Fig. S2.

Considering the evolution of the random walk under the effect of time independent gauge field, Fig. S3 summarizes the numerical results for the variation of quadratic means with time step for different values of ϕ . The obtained results show that how such a gauge field can affect quadratic means of x and y to be decreased relative to the zero phase modulation case. Note that these quadratic means are normalized relative to the total power in the up and down channels.

Non-uniform modulation:

We next consider the case in which the phase modulation pattern changes across a boundary. This type of phase modulation can lead to the emergence of the edge states right along the boundary. Here, we have considered $y = 0$ as the boundary separating two time independent linear phase modulations in $y > 0$ and $y < 0$. Since we do not have translational symmetry in y direction anymore, we cannot define k_y for this configuration. However, we can still obtain the allowed eigen-energies for different k_x values. In order to obtain these eigen-energies, we should obtain the

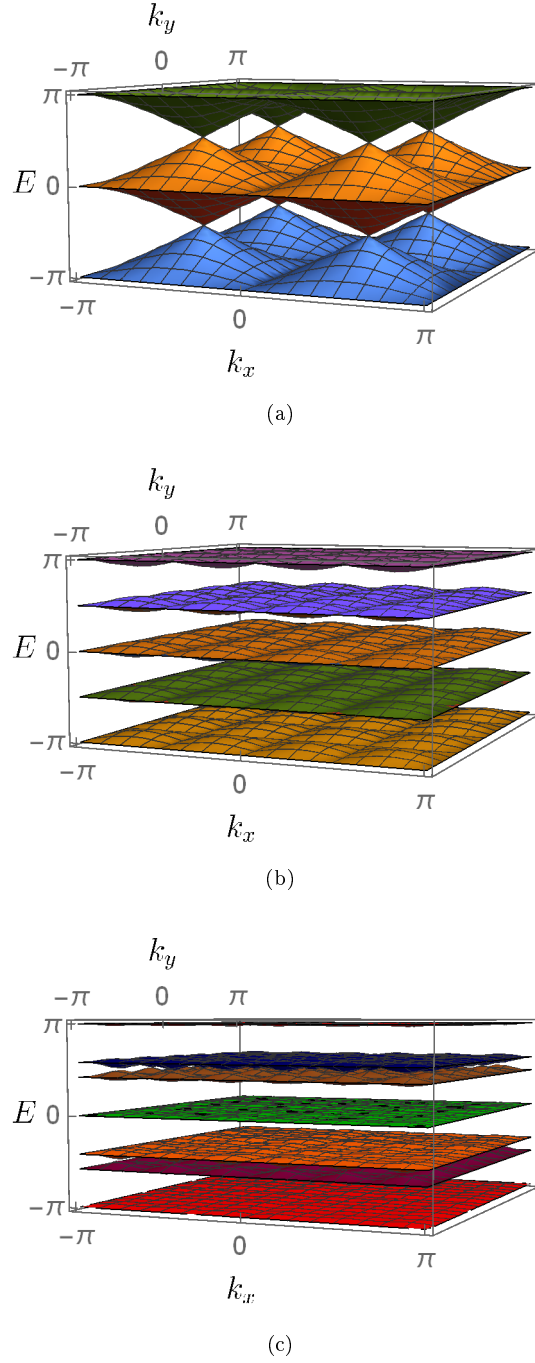
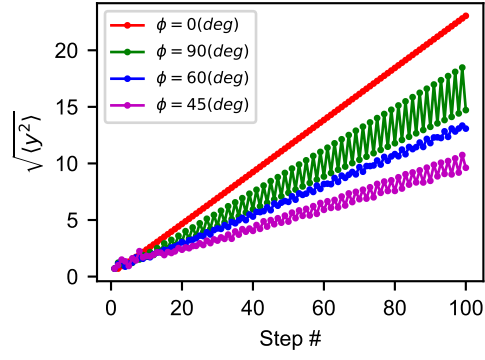


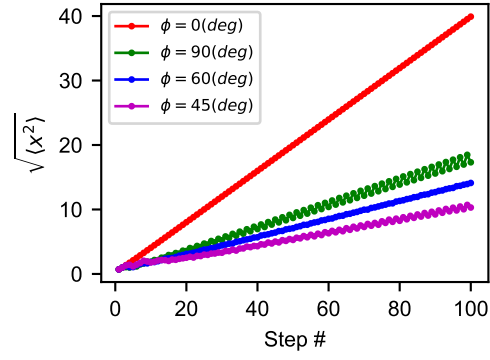
Figure S2. The energy band diagrams for the time independent phase modulation with (a) $\phi = \pi$ and (b) $\phi = \pi/2$ and (c) $\phi = \pi/3$.

propagation matrix in the real space under the appropriate boundary conditions. Depending on the phase modulations at the top (ϕ_T) and the bottom (ϕ_B), we obtain different band diagrams. Numerical results show that if one of ϕ_T and ϕ_B be zero then there exists no edge states. Moreover, the edge states exist only if $0 < \phi_T < \pi$ & $-\pi < \phi_B < 0$ or $0 < \phi_B < \pi$ & $-\pi < \phi_T < 0$.

We have plotted the energy band diagrams as functions of k_x momentum for different ϕ_T and ϕ_B in Fig. S4. In this figure, we have considered different cases of $\phi_T = -\phi_B$ as non-uniform configurations with a boundary separating two different linear phase modulations. Note that swapping the values of ϕ_T with ϕ_B will modify the band diagram by replacing the edge states with the ones that propagate in the reverse direction. We have also shown the band



(a)



(b)

Figure S3. (a) The quadratic mean of y and (b) the quadratic mean of x as a function of time step for different values of phase modulations.

diagrams corresponding to uniform modulations with $\phi_B = \phi_T$ for comparison.

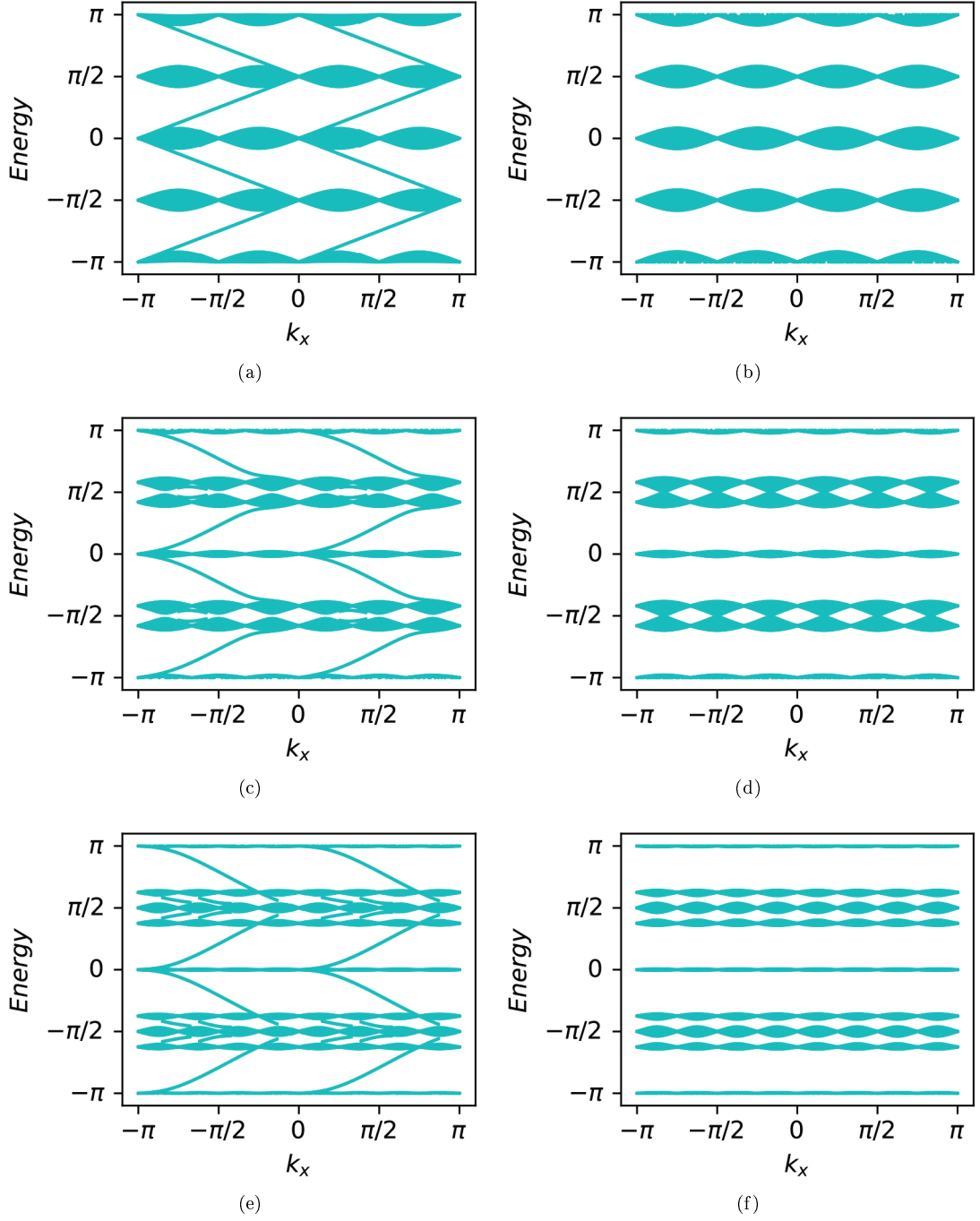


Figure S4. The left panel shows the energy band diagrams for the time independent non-uniform phase modulations of (a) $\phi_T = -\phi_B = \pi/2$ and (c) $\phi_T = -\phi_B = \pi/3$ and (e) $\phi_T = -\phi_B = \pi/4$. The right panel shows the corresponding band diagrams for the uniform phase modulations of (b) $\phi_T = \phi_B = \pi/2$ and (d) $\phi_T = \phi_B = \pi/3$ and (f) $\phi_T = \phi_B = \pi/4$.